NJC

Accepted Manuscript

This article can be cited before page numbers have been issued, to do this please use: S. K. Hadjikakou, C. N. Banti, N. Kourkoumelis, C. Raptopoulou and V. Psycharis, *New J. Chem.*, 2017, DOI: 10.1039/C7NJ01117B.

ROYAL SOCIETY OF CHEMISTRY

rsc.li/njc

View Article Online
DOI: 10.1039/C7NJ01117B

Journal Name

ARTICLE

N-(4-hydroxyphenyl)acetamide against di-iodine towards polyiodide dianion

Received 00th January 20xx,
Accepted 00th January 20xx

DOI: 10.1039/x0xx00000x

www.rsc.org/

Christina N. Banti[a]*, Nikolaos Kourkoumelis[b], Catherine P. Raptopoulou [c], Vassilis Psycharis[c], Sotiris K. Hadjikakou[a]*

The direct reaction of *N*-(4-hydroxyphenyl)acetamide or paracetamol ($C_8H_9NO_2$, PACET), a widely used Non Steroidal Anti-Inflammatory Drug (NSAID), with di-iodine forms the ionic salt of formula $\{[(PACET)_2H^+]_2\cdot(I_8)^{2-}\}$ (**1**) with the simultaneous reduction of iodines to iodides. The compound was characterized by X-ray diffraction analysis. Compound **1** contains the polyiodide $(I_8)^{2-}$ counter di-anions, in z-shape conformation. By taking into account secondary I···I interaction the shape turns to be rectangular. Moreover, *N*-(4-hydroxyphenyl)acetamide inhibits the catalytic activity of horse radish peroxidase (HRP) (a model of Thyroid Peroxidase (TPO)) on the oxidation of iodides to di-iodine by hydrogen peroxide, as evidence of the kinetic and computational studies. The inhibition activity of PACET against the catalytic oxidation of iodides by H_2O_2 in the presence of FeTPPCl (a model of the active site of TPO) is measured as a result of the yield of I_3^-.

Introduction

Eu-thyroid sick syndrome is the low concentration of thyroid hormones in the plasma which is occurring without dysfunction of the thyroid gland. It has been proposed that drugs such as furosemide, fenclofenac, carbamazepine or salicylate compete with the binding of thyroid hormone to plasma proteins; causing a decrease of total triiodothyronine T3 and its prohormone tetraiodothyroxine T4 hormones [1]. The synthesis of thyroid hormone, T3 and T4, on the other hand, follows the oxidation of iodides to di-iodine by the enzyme Thyroid Peroxidaze (TPO) (Scheme 1). TPO, an iron-porphyrin enzyme [2] is responsible for the oxidation of iodide anions [2b,3]. Tyrosil residues of thyroglobuline, a protein rich in tyrosine, are iodinized to form mono-iodotyrosine (MIT) or di-iodiotyrosine (DIT). Compensation reaction among these intermediates results the prohormone T4. Deiodination of T4 by the selenoenzyme thyroid deiodinase (ID-1-SeH) leads to the formation of the active hormone T3. The thyroid hormones formation is summarized in scheme 1 [2-7].

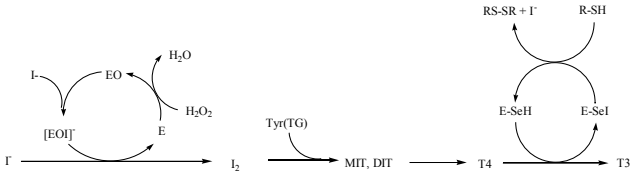

Scheme 1. Mechanism of TPO catalyzed iodination reactions. (MIT= 3-mono-iodo-tyrosine and DIT= 3,5-di-iodo-tyrosine E= TPO-TPP-Fe, EO= TPO-TPP-Fe=O, [EOI]-= [TPO-TPP-Fe=OI]-, TPP= tetraphenyl-porphyrine, E-SeH= thyroid deiodinase, RSH= glutathione)

Moreover, Horse Radish Peroxidase (HRP) is an important heme-containing enzyme that utilizes hydrogen peroxide to oxidize a wide variety of organic or inorganic compounds [8a]. HRP catalyzes oxidation of iodides to di-iodine by hydrogen peroxide [8b]. Therefore, HRP can be used as a model of TPO [8c]. Moreover, animals' peroxidases display high sequence homology compared to plant peroxidases [8d].

N-(4-hydroxyphenyl)acetamide or paracetamol is a common NSAID. Nowadays, it is among the best seller medication for its analgesic and antipyretic properties, worldwide [9]. Since early 80's, clinical trials were pointed out the interference in absorption, distribution and elimination of PACET in patients before and after treatment of

[a] *Section of Inorganic and Analytical Chemistry, Department of Chemistry, University of Ioannina, 45110 Ioannina, Greece;*
[b] *Medical Physics Laboratory, Medical School, University of Ioannina, Greece;*
[c] *NCSR "Demokritos", Institute of Nanoscience and Nanotechnology, 15310, Aghia Paraskevi Attikis, Greece.*

* All correspondence should be addressed to:
Dr. C.N. Banti (Post Doctoral Fellow); email: cbanti@cc.uoi.gr
Dr S.K. Hadjikakou (Professor); e-mail: shadjika@uoi.gr;
tel. xx30-26510-08374
fax xx30-26510-08786
Electronic Supplementary Information (ESI) available: [details of any supplementary information available should be included here]. See DOI: 10.1039/x0xx00000x

View Article Online
DOI: 10.1039/C7NJ01117B

hypothyroidism [9a]. A decrease in *N*-(4-hydroxyphenyl)acetamide elimination during hypothyroidism, without the estimation of the metabolic clearance was observed [10]. Moreover, the metabolism of N-(4-hydroxyphenyl)acetamide by glucuronidation is decreased in case of severe hypothyroidism [10b].

During our studies on the perturbation of the I-I bond when diiodine interacts with heterocycles [6,7,11] such as *N*-(4-hydroxyphenyl)acetamide (Scheme 2) leads in the isolation of $\{[(PACET)_2H^+]_2\cdot(I_8)^{2-}\}$ (**1**). Compound **1** was characterized by X-ray diffraction analysis. The formation of **1** demands the reduction of di-iodine to octa-iodide di-anion. The significance of **1** in the interfering mechanism of TPO-catalyzed iodination reactions of tyrosil residues of thyroglobuline, is also reported. This interference is further investigated by the study of the inhibition activity of PACET against the enzyme HRP. The results are compared with those obtained from its implementation on the catalytic oxidation of iodides by H_2O_2 in the presence of FeTPPCl. In this case the yield of I_3^- derives from the oxidation of I^-. Molecular modeling studies were carried out to gain structural insight and propose a valid binding model for the HRP- *N*-(4-hydroxyphenyl)acetamide complex.

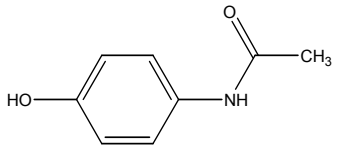

Scheme 2. *N*-(4-hydroxyphenyl)acetamide

Results and Discussion

Synthesis: The reaction between PACET and I_2 in 1:1 molar ratio in dichlomethane leads to the formation of **1** (Scheme 3). Compound **1** consists by two cationic $[(PACET)_2H^+]$ species and one dianionic $(I_8)^{2-}$ counter part. While the octa-iodide dianion is formed by the reduction of di-iodine, the protons are released from hydroiodic acid derived form the reaction of di-iodine with water traces of the solvent (Scheme 3) [12].

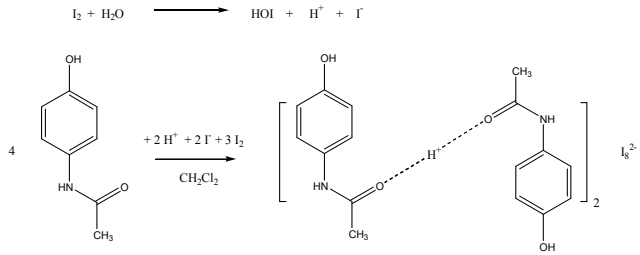

Scheme 3

Crystal and molecular structure: Structures containing polyiodide anions with cationic aromatic complexes as counterparts are rare in the literature. Although the asymmetric unit cell consists of two symmetry independent partially protonated $(PACET)(H^+)_{0.5}$ cations, one $(I_3)^-$ anion and half of I_2 diodine molecules, the molecular diagram of 1 is better described as shown in Figure 1A, i.e. $\{[(PACET)_2(H^+)][(PACET)_2(H^+)]'\cdot(I_3)_2^-(I_2)\}$ or $\{[(PACET)_2(H^+)]_2\cdot(I_8)^{2-}\}$.

Figure 1

Compound **1** contains $[I_8]^{2-}$ dianions. Usually, the configuration of $[I_8]^{2-}$ dianions is (a) consisted by two $[I_3]^-$ ions that are connected through the end atoms by an I_2 ($([I_3]^-)_2\cdot[I_2]$) while (b) the configuration $([I_5]^-)\cdot([I_3]^-)$ is also reported [13]. The geometries which are observed by octa-iodide dianions are either (i) Z-shape, (ii) V-shape, (iii) L-shape or (iv) linear [13]. For the iodine-iodine bonds or contacts observed in **1** and listed below the corresponding definitions given in ref. [13] are used [r1, r2, r3, r4, r5, r6, r7 for bonds and contacts and α1,α2, α3, α4, α5, α6 for angles, Table 5, Figure 20 of ref. [13]]. The I1-I2, I2-I3 {r2, r1 correspondingly and r6, r7 for the symmetry equivalent I1*-I2*, I2*-I3*, [symmetry code: (*):1.5-x,y, 0.5-z]} bond lengths in **1** are 3.0077(3) and 2.8493(3) Å respectively indicating slightly asymmetric I_3^- (Figure 1A). The I1···I4 (r3 and r5 for the symmetry equivalent one I1*···I4*, Figure 1A) distance (3.3612(4) Å) which is shorter than the sum of van der Waals radii of two iodine atoms (I···I van der Waals bond length is extend up to 4.20-4.44 Å [14]) bridge the ends of two I_3^- species with the I_2 moieties leading to the formation of the $[I_8]^{2-}$ units. The I4-I4* bond length (r4 parameter in octaiodide units) is 2.7509(4) Å slightly longer than that of neutral di-iodine (gas phase: 2.677 Å [15] crystal: 2.715 Å at 110 K [15] due to the interaction with two $[I_3^-]$ moieties. Thus, the configuration of octaiodide dianion in **1** is $[I_3]^-\cdot[I_2]\cdot[I_3]^-$ with Z-shape and possess a 2-fold axis passing through the middle of the I4-I4* bond (Figure-1a). The lengths of the parameters defining the Z-shaped octa-iodide units are in good agreement with those listed in ref [13] (Table 5) but differences are observed in the corresponding angles. The angle values for **1** I1-I2-I3 [=175.845(9)^o (=I1*-I2*-I3*), α1/α6 (in ref. 20)], I2-I1-I4 [=94.54^o(1)(= I2*-I1*-I4*), α2/α5 (in ref. [13])] and I1-I4-I4* [=169.68(1)(= I1-*I4*-I4, α3/α4 (ref.[13])] take values closer to those for compound $[Cu(phen)_2I]_2I_8$ with the highest deviation to be observed for the α3/α4 angles. The octa-iodide units are arranged in layers parallel to the (010) planes as shown in Figure 1B, resulting in a pattern which is observed, for first time to the best of our knowledge. The octa-iodide units are considered as the building blocks of the layered structure based on the hierarchy of intermolecular interactions for polyiodide compounds suggested by Svensson et.al [13]. The values given above for the bonds within the I_3^- and I_2 units are in agreement with the literature data for intramolecular iodine atom interactions and the distances I1···I4* (dashed magenta lines in Figure 1B) are in the range of what is considered as secondary bonds [13]. The dashed orange I4···I3***[=3.8462(5) Å (=I4*···I3**), symmetry code: (**): 1-x, -y, -z; (***): 0.5+x, -y,

View Article Online
DOI: 10.1039/C7NJ01117B

0.5+z] and the dashed green I1···I2#[=4.2334(5) Å (=I2···I1#), symmetry code: (#): 0.5+x, -y, 0.5+z] lines in Figure 1B indicate intermediate and weak van der Waals interactions respectively. Those of the first type results in the formations of stripes of octaiodide units parallel to the [101] crystallographic direction and those of the second type are developed along the [100] direction and built the layers which are described by the formula $_{\infty}^{2}[I_3 \cdot I_2 \cdot I_3]^{2-}$.

The charge of the octaiodide units is counterbalanced by four partially protonated $(PACET)(H^+)_{0.5}$ moieties which are shown in Figure 1A and they consist of pairs of PACET molecules which share two hydrogen atoms located on inversion centers, H3O is on (0.0,0.5,0.5) and H1O is on (1.0,0.0, 0.0) centre of symmetry. These type of intermolecular interactions are characterized by the long O-H bonds [H1O-O1= H1O-O1''=1.210(2) Å and H3O-O3=H3O-O3'= 1.214(2) Å] and short O···O distances [2.420(4) Å for O1···O1' and 2.419(4) for O3···O3' Å] [16]. The pairs of partially protonated PACET molecules interact with each other through the hydrogen bond O2-H2O···O4 (Figure 1A, Table 1) and form chains parallel to the [201] crystallographic direction. The protonated ligand is in its keto form. The C–O bond length found in **1** are O1-C2= 1.267(3) and O3-C10= 1.267(3) Å slightly longer of the C-O bond found in free *N*-(4-hydroxyphenyl)acetamide (1.224 Å [17]) due to the protonation. This also affects the N-C(O) bond lengths with two shorter N1-C2= 1.321(4) and N2-C10= 1.325(3) Å and two longer ones N1-C3= 1.434(3) and N2-C11= 1.424(3) Å. Therefore the bond and charge distribution is shown in scheme 4.

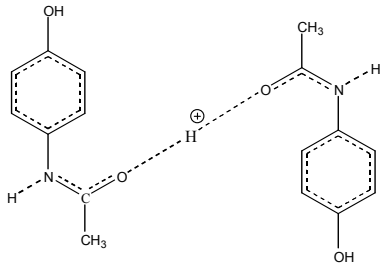

Scheme 4. Bond and charge distribution in **1**.

Table 1

The chains of pairs of partially protonated PACET molecules are stacked along the [101] direction and they interact through π-π interactions with centroid distances 3.7568(1) and 3.6101(1) Å for Cg1···Cg1[II] and Cg2···Cg2[III] respectively (Cg1 and Cg2 are the centroids of C3…C8 and C11…C16 phenyl rings, symmetry code: (!!): 1.5-x, y, 0.5-z; (!!!):0.5-x, y,0.5-z) thus forming layers parallel to the (010) plane lying above the layers of polyiodide layers as shown in Figure 2A. The PACET molecules forming the layers interact further through the O4-H4O···I1, N1-H1N···I3 and N2-H2N···I2 hydrogen bonds (Figure 1A, Table 1) with the atoms of the polyiodide layers lying above and below, thus contributing to the formation of the 3D architecture for **1** (Figure 2B).

Figure 2

Peroxidase-catalysed iodide oxidation: In order to ascertain the mechanism of interference of *N*-(4-hydroxyphenyl)acetamide on the thyroid hormone synthesis (Scheme 1) the inhibitory activity of the drug on Horse Radish Peroxidase (HRP) is studied. The HRP has well known spectral properties and is an appropriate tool for the study of the influence of drugs on the iodide oxidation by H_2O_2 and consequently of the thyroid hormone formation [18]. Peroxidase-catalysed iodide oxidation was monitored at 353 nm following the formation of I_3^-. The assay includes: 1.7 mM KI, 1.8 nM HRP and 10 mM H_2O_2 in 50 mM sodium acetate buffer (pH= 5.5) in a final volume of 2 ml [19a]. Figure 3 shows the HPR activity (A%) versus various concentrations of PACET. The antithyroid drugs of clinical use, methimazole (MMI) and 6-n-propyl-thiouracile (PTU) were used for comparison. MMI and PTU are known to inhibit TPO [7]. The degree of HRP activity (A, %) in the presence of PACET, MMI and PTU is calculated from the equation

$$A(\%) = \frac{\tilde{o}_i \text{ in the presence of the drug}}{\tilde{o}_i \text{ in the absence of drug}} \quad 100$$

where υ_0 is the initial rate.
While the value of the initial rate (υ_0, mM s^{-1}) is derived from the equation:

$$\tilde{o}_i = \frac{\ddot{A}C}{\ddot{A}t} = \frac{\ddot{A}\acute{A}}{\mathring{a}\,\ddot{A}t} = \frac{tg\,a}{\mathring{a}}$$

where C is the product concentration (I_3^-), t is the reaction time, ε is the molar absorption coefficient, of I_3^- (25550 M^{-1} cm^{-1}), tg a is the slope of the kinetic curve plotted as absorbance vs time.

Figure 3

The IC_{50} value of the inhibitory activity of *N*-(4-hydroxyphenyl)acetamide towards HRP catalytic activity on the oxidation of iodides by H_2O_2 is 43.9 μM. The corresponding values of the antithyroid drugs MMI and PTU are: 18.9 and 27.8 μM, respectively. Although, the activity for paracetamol plateaus at 40% (Figure 3), contrary to the MMI and PTU, the higher inhibitory concentrations of PACET are used to construct the concentration – response plot in order to determine the IC_{50} value accurately [19b]. One common caused is the low compound solubility at the higher concentrations. Despite the lower inhibitory activity of PACET towards MMI and PTU against HRP, the reductance of the concentration of the active di-iodine through chemical reaction (see x-ray analysis) should be taken into consideration as well. Thus, PACET depresses the total amount of the active di-iodine available for the iodination of tyrosil residues of thyroglobulin.

View Article Online
DOI: 10.1039/C7NJ01117B

The reversible type of inhibitor was tested by incubating the enzyme with the inhibitor, PACET at a concentration equal to its IC_{50}, before adding the KI and H_2O_2 at different periods of time (0-10 min). The incubating time showed no influence on enzyme activity, suggesting a reversible type of inhibition (Figure S1) [20]. The corresponding data of MMI and PTU are also shown for comparison.

The inhibition mechanism caused by PACET on the enzymatic reaction was studied by steady-state kinetics at various substrate concentrations (varied from 10 to 70 mM) in the absence and presence of drug. The experimental data were processed by a graphical method in Lineweaver–Burk coordinates (double reciprocal method) (Figure S3). The kinetic parameters K_m and V_{max} were estimated from the slope and intercept of the line [21] (Figure S3) Control experiments were also performed. The experimental data for the PACET are plotted in Figures 4 and S3. The K_m and V_{max} values for the PACET, are 113 mM and 4.95×10^{-3} mM/sec, respectively in contrast to the corresponding one of the enzyme HRP (K_m= 498 mM and V_{max}= 25×10^{-3}) mM/sec. For comparison the corresponding K_m and V_{max} values of MMI and PTU are 153 mM and 1.3×10^{-3} mM/sec ((MMI) and 108 mM and 7.4×10^{-3} mM/sec (PTU) respectively (Figure 4). Therefore, both K_m and V_{max} values were decreased upon incubation of the enzyme with the inhibitors PACET, MMI or PTU indicating that they inhibit HRP with an uncompetitive mechanism. Thus, PACET inhibits the enzyme with a similar way with its inhibitors MMI and PTU. In this mechanism, the EI (enzyme-inhibitor) is not formed, but only the ESI (enzyme-substrate-inhibitor). This occurs when the inhibitor binds to a site which only becomes available following the substrate bound to the active site of the enzyme [21].

Figure 4

Inhibition of the catalytic activity of FeTPPCl: Since HRP contains iron(III) protoporphyrin IX (the 'heme group') in its active site, the catalytic oxidation of iodide by H_2O_2 in the presence of ferric tetra-phenyl-porphyrin chloride (FeTPPCl) was studied experimentally [8a].

The absorption spectra of I_3^- species show maxima at 288 nm and 353 nm [22]. The formation of the I_3^- species was assayed by their absorbance at 353 nm [7,22] given that neither PACET, MMI, PTU nor KI absorb at this wavelength (Figure S2). Measurements were performed at room temperature using solutions in a mixture of dichloromethane and methanol 60:40 by volume. The assay system contained KI= 10 mM, [H_2O_2]= 0.125 mM, [FeTPPCl]= 0.01 mM, [L]= 0.1 mM (L= pacet, MMI, PTU). The volume was adjusted to the total of 2 ml in the cell. The use of an excess of iodide is to ensure the complete conversion of all the di-iodine formed from oxidation of iodide by H_2O_2 into tri-iodide [23]. Also an excess of I^- is needed since at a concentration below of 10 mM no I_3^- or I_2 could be detected spectroscopically [24].

The reaction of KI in the presence of H_2O_2 results I_3^- in 50% yield while in the presence of the catalyst [FeTPPCl] the yield rise up to 98% [23]. Hence, 100% production of I_3^- is equivalent to a concentration of 50 μM of I_3^- which corresponds to the maximum amount of H_2O_2 consumed in this reaction [7]. The inhibition percent is calculated by the difference between the maximum amount I_3^- (KI, H_2O_2, FeTPPCl) and that formed in the presence of PACET.

Figure 5 illustrates the effect caused by PACET in the catalytic activity of FeTPPCl. Although MMI and PTU are poisoning the catalyst FeTPPCl by decreasing the yield of I_3^- by 25.5 and 7.8 %, respectively [7], PACET, on the contrary, acts as co-catalyst by increasing the amount of the reaction product (Figure 5). This observation seems to contradict the inhibitory activity towards HRP caused by PACET (See above). However, the involvement of the Pro139 residue in the active site of HRP as evidence of crystallographic data plays a crucial role in the active site conformation [8a] (see also molecular modeling studies below) the reaction is repeated in the presence of equimolar amounts of PACET and Fmoc-Pro-OH. The yield of I_3^- in this case is decreased by 33.1 % relatively to the maximum which is achieved from the initial reaction (KI, H_2O_2, FeTPPCl). Therefore PACET acts as HRP inhibitor by acting in its active site.

Figure 5

Molecular modeling study: Molecular modeling studies were carried out to gain structural insight and propose a valid binding model for the HRP-PACET complex. The unbound HRP structure (PDB ID: 1H5G, resolution: 1.6 Å) [25] was used as the receptor. The experimental structure of the complex HRP-benzhydroxamic acid (PDB ID: 2ATJ, resolution: 2.0 Å) [26] shows small differences between the bound and unbound states and therefore was used to verify the docking site [27] and the subsequent study of the complex dynamics. Molecular docking studies involved 500 runs; the results were clustered into 6 distinct complex conformations different by at least 5 Å heavy atom RMSD. Rank 1 group consists of 64% of all conformations having the lowest average free energy of binding (-5.1 ± 0.3 kcal/mol) residing in the cavity formed by Arg38, His42, Phe68, Gly69, Ser73, Leu138, Pro139, Ala140, Pro141, Phe142, Phe179, and hem350. Figure 6 shows the top ranked pose of *N*-(4-hydroxyphenyl)acetamide with the unbound HRP structure superimposed to the 2ATJ (bound) structure.

Figure 6

Normally, the oxo group of *N*-(4-hydroxyphenyl)acetamide can occupy the corresponding space of the acetoxy group of benzhydroxamic acid (BHA) being 1.67 Å closer to heme. Molecular docking results cannot exclude the possibility of allosteric sites since the calculated binding energies of the other poses are in the range of -4.8 to -4.5 kcal/mol and include poses away from the active site (for example at the vicinity of Thr200, Tyr201 Thr204, Leu223, and Lys241).

The stability of the most favored, by energetic terms, HRP-PACET complex was subsequently studied by 12 ns molecular

View Article Online
DOI: 10.1039/C7NJ01117B

dynamics (MD) simulation followed by trajectory analysis. Validation of the docking pose using MD is generally considered as a crucial step towards the analysis of the dynamic behavior of the protein-ligand complex since many studies have shown that a ligand in its best docking pose can "fly away" during an MD simulation [28]. When the ligand was subjected to MD simulation, its position and orientation in the binding cavity was only slightly changed. Specifically, the RMSD between the docked pose and the minimum energy MD structure was found to be 0.84 Å which is attributed to the translational motion by ~1 Å towards heme. *N*-(4-hydroxyphenyl)acetamide is stabilized in the HRP active site by significant hydrophobic interactions (Figure 7, red spokes) and hydrogen bonding interaction between the N atom of ligand and Pro139 (2.88 Å) similarly with BHA in the 2ATJ structure (2.71 Å). The most significant, i.e. less than 4 Å, non-bonded contacts were between the ligand and Pro141 (3.49 Å), Ala140 (3.83 Å). An extended interaction between *N*-(4-hydroxyphenyl)acetamide and the distal heme (4.58 Å) is possible and analogous to 2ATJ through an extended hydrogen bonding network via the oxo moiety. The lack of peripheral hydrophobic cavity suggests that the active site can host aromatic substrates near heme but with no access to the ferryl-oxygen. [26]

Figure 7

By excluding the first ns of the simulation as the equilibrium period we calculated the mean binding energy of the ligand to be -5.2 kcal/mol. Although this value is close to the corresponding docking one, we must note that Vina docking procedure is force field independent while MD tasks evaluate potential force field energies; thus, a direct comparison is not necessarily representative. In accordance with other studies of *N*-(4-hydroxyphenyl)acetamide towards similar (i.e., containing the heme moiety) macromolecular targets, PACET forms weakly bound protein–ligand complexes. [29-31]. In this view, x-ray and MD data are consistent regarding ligand binding affinity although we cannot exclude the possibility of multiple binding poses.

The stability of the unbound HRP and the corresponding HRP-PACET complex was studied by examining the root mean square deviation (Cα-RMSD). Moreover, the root mean square fluctuation (RMSF) was calculated to assess the flexibility of the system under the specified computational parameters (Figure S4).

The minimal conformation change that is shown in Figure 8 [32] for the HRP-PACET complex corroborates with the crystallographic solution of the 2ATJ structure where the structures of the bound and unbound states are comparable. Similarly, minimal structural rearrangement is observed in response to *N*-(4-hydroxyphenyl)acetamide binding. The presence of possible allosteric sites combined with the insignificant protein conformational change upon complexation, especially in the region of the active site.

Figure 8

Conclusions

Compound **1** contains the octa-iodide $[I_8]^{2-}$ dianions. The configuration of $[I_8]^{2-}$ dianions is consisted by two $[I_3]^-$ ions that are connected through the end atoms by an I_2 (($[I_3]^-$)$_2$·$[I_2]$), with Z-shape geometry. Two sequential Z-shaped octa-iodides form 10-member rings through the interaction of the di-iodides with triiodide ions (Figure 1b). The contact distance between the iodine atoms is 3.846 Å (Figure 1b). This architecture is rare and to our knowledge **1** is the first example of 10-member rings growth from Z-shape octa-iodides building blocks. However, 18-member rings from octa-iodides are already known [13].

The isolation and characterization of **1** by the direct reaction between PACET and (active) di-iodine premise the reduction of di-iodine to octa-iodide di-anion. Additionally, PACET inhibits the activity of HRP towards the formation of the di-iodine in a similar manner with the antithyroid drugs MMI and PTU. Thus, PACET not only reduces the concentration of the active di-iodine (see X-ray analysis) but it also inhibits HRP activity, by uncompetitive mechanism. The study of the catalytic activity of FeTPPCl in the iodide oxidation reaction by H_2O_2 under the presence of Fmoc-Pro-OH confirms the inhibitory activity of PACET, sicne Pro141 (3.49 Å), was pointed out by computational studies to exhibit the most significant non-bonded contacts with the PACET.

Experimental

Materials and instruments: All solvents used were of reagent grade. Solvents used were of reagent grade, while horse radish peroxidase, *N*-(4-hydroxyphenyl)acetamide, 6-*n*-propyl-2-thiouracil, methimazole, ferric tetra-phenyl-porphyrin chloride, KI, H_2O_2 (Sigma-Aldrich, Merck) were used without further purification. Melting points were measured in open tubes with a Stuart Scientific apparatus and are uncorrected. A UV-1600 PC series spectrophotometer of VWR was used to obtain electronic absorption spectra.

*Synthesis and crystallization of **1**:* 0.5 mmol paracetamol (0.076 g) and 0.5 mmol I_2 (0.127 g) was mixed and stirred in 15 mL dichloromethane for 2 hours at 0^{o}C temperature. Red crystals of **1** suitable for X-ray analysis were grown from slow evaporation of the solution after 7 days.

1: Red crystals, Yield: 0.055 g; melting point: 114-116 °C; Elemental analysis found: C: 23.53; H: 2.32, N: 3.23 %; calculated for $C_{16}H_{19}I_4N_2O_4$: C: 23.70; H: 2.36; N: 3.34 %.

X-ray Structure Determination: Crystals of compound **1** (0.18x0.23x0.24 mm) were cooled to -113 ^{o}C for data collection. Diffraction measurements were made on a Rigaku R-AXIS SPIDER Image Plate diffractometer, using graphite-monochromated Mo-Ka (λ = 0.71073 Å) radiation. Data collection (ω-scans) and processing (cell refinement, data reduction and Empirical absorption correction) were

View Article Online
DOI: 10.1039/C7NJ01117B

performed using the CrystalClear program package [33]. The structure was solved with direct methods with SHELXS-97 [34] and refined by full-matrix least-squares procedures on *F*2 with SHELXL 2014/6 [35]. Hydrogen atoms were located by difference maps and were refined isotropically or were introduced at calculated positions as riding on bonded atoms. All non-hydrogen atoms were refined anisotropically.

1: $C_{16}H_{19}N_2O_4I_4$ MW= 810.93, monoclinic, space group P2/n, a= 14.1757(6) Å, b= 9.6136(3) Å, c= 17.0845(6) Å, α= 90 º, β= 97.777(2) º, γ= 90 º, V= 2306.85(15) Å^3, Z= 4, T= 160 K, ρ (calc)= 2.090 g cm^{-3}, μ= 5.43mm^{-1}, F(000)= 1492. $2\vartheta_{max}$ = 54°; reflections collected/unique/used, 14491/5000 [R_{int} = 0.035]/5000; 289 parameters refined; $(\Delta/\sigma)_{max}$= 0.004; $(\Delta\rho)_{max}/(\Delta\rho)_{mi}$ = 1.59/-0.46 e/Å^3; s=1.05; *R*1/w*R*2 (for all data), 0.0264/0.0557; *R*1/w*R*2 (for 4551 reflections with $I > 2\sigma(I)$), 0.234, 0.0543 [$w = 1/[\sigma^2(F_o^2) + (0.0234P)^2 + 1.0336P]$ where $P = (F_o^2 + 2F_c^2)/3$].

Crystallographic data for the structures reported in this paper have been deposited with the Cambridge Crystallographic Data Centre as supplementary publication no. CCDC- 1522200 (**1**). Copies of the data can be obtained free of charge on application to CCDC, 12 Union Road, Cambridge CB2 1EZ, UK (fax: (+44) 1223-336-033; e-mail: deposit@ccdc.cam.ac.uk).

In silico studies: Molecular docking and dynamics simulations were performed with YASARA structure (v16.9.23) software package [35]. Global docking was performed using AutoDock VINA [36] within an adequate volume covering the whole protein space using the default parameters exposed by the YASARA interface [37]. The best ranked pose was used as the starting point for the subsequent MD study. For HRP unbound and complex systems a 12 ns MD simulation was carried out at 298 K (NPT ensemble) followed by energy minimization and calculation of the interaction energy for the HRP-paracetamol complex. Simulations were performed in a boundary periodic cell of 85.24^3 Å solvated with TIP3P water molecules with a maximum sum of all bumps per water of 1.0 Å and density of 0.997 g/mL with explicit solvent. Residue protonation states were assigned based on the calculated pKa values at pH 7.4 [38]. The cell was neutralized to 0.9% NaCl ion mass fraction corresponding to physiological condition. The AMBER14 force field [39] was used and long-range Coulomb interactions were assessed using particle-mesh Ewald (PME) summation [40-41] and a cut-off of 8.0 Å. The ligand, paracetamol, was selected from PDB (PDB ID: 1TYL) and was optimized before the simulations with the semi-empirical PM3 parameterization scheme.

References

1 M.H. Warner, G.J. Beckett, J. Endocrinol., 2010, 205, 1–13
2 (a) P.J. O'Brien, Chem.-Biol. Interact., 2000, 129, 113–139. (b) A.B. Rawitch, A. Taurog, S. B. Chernoff, M.L. Dorris, Arch. Biochem. Biophys., 1979, 194, 244–257.
3 (a) R.P. Magnusson, A. Taurog, M.L. Dorris, J. Biol. Chem., 1984, 259, 197–205. (b) R.P. Magnusson, A. Taurog, M.L. Dorris, J. Biol. Chem., 1984, 259, 13783–13790. (c) M. Huwiler, U. Burgi, H. Kohler, Eur. J. Biochem., 1985, 147, 469–476. (d) P.N. Jayaram, G. Roy, G. Mugesh, J. Chem. Sci., 2008, 120, 143–154. (e) S. Mondal, K. Raja, U. Schweizer, G. Mugesh, Angew. Chem. Int. Ed. 2016, 55, 7606 –7630
4 M.C. Aragoni, M. Arca, F. Demartin, F.A. Devillanova, A. Garau, F. Isaia, V. Lippolis, G. Verani, J. Am. Chem. Soc., 2002, 124, 4538–4539
5 W.W. du Mont, G. Mugesh, C. Wismach, P.G. Jones, Angew. Chem., Int. Ed., 2001, 40, 2486–2489
6 C.D. Antoniadis, G.J. Corban, S.K. Hadjikakou, N. Hadjiliadis, M. Kubicki, S. Warner, I.S. Butler, Eur. J. Inorg. Chem. 2003, 1635-1640,
7 G.J. Corban, S.K. Hadjikakou, A.C. Tsipis, M. Kubicki, T. Bakas, N. Hadjiliadis, New J. Chem., 2011, 35, 213–224
8 (a) N.C. Veitch, Phytochemistry, 2004, 65, 249-259, (b) P.F. Hollenberg, T. Rand-Meir, L.P. Hager, J. Biol. Chem, *1974,*. 249, 5816-5825, (c) R.J. Maguire, H.B. Dunford, Biochemistry, 1972, 11, 937–941, (d) F. Bafort, O. Parisi, J.-P. Perraudin, M.H. Jijakli, Enzyme Research, 2014, Article ID 517164
9 (a) E.M. Lancaster, J.R. Hiatt, A. Zarrinpar, Arch Toxicol, 2015, 89, 193–199, (b) C.N. Banti, S.K. Hadjikakou, Eur. J. Inorg. Chem. 2016, 3048–3071
10 (a) J.C. Forfar, A. Pottage, A.D. Toft, W.J. Irvine, J.A. Clements, L.F. Prescott, Eur J Clin Pharmacol., 1980, 18, 269-273, (b) J. Sonne, S. Boesgaard, H. Enghusen Poulsen, S. Loft, J. Molholm Hansen, M. Dossing, F. Andreasen, Br. J. clin. Pharmac., 1990, 30, 737-742
11 (a) V. Daga, S.K. Hadjikakou, N. Hadjiliadis, M. Kubicki, J.H.Z. dos Santos, I.S. Butler, Eur. J. Inorg. Chem. 2002, 1718-1728, (b) J.H.Z. dos Santos, I.S. Butler, V. Daga, S.K. Hadjikakou, N. Hadjiliadis, Spectrochim. Acta Part A, 2002, 58, 2725–2735, (c) C.D. Antoniadis, S.K. Hadjikakou, N. Hadjiliadis, M. Kubicki, I.S. Butler, Eur. J. Inorg. Chem. 2004, 4324-4329, (d) C.D. Antoniadis, S.K. Hadjikakou, N. Hadjiliadis, M. Kubicki, I.S. Butler, New J. Chem., 2005, 29, 714–720, (e) G.J. Corban, S.K. Hadjikakou, N. Hadjiliadis, M. Kubicki, E.R.T. Tiekink, I.S. Butler, E. Drougas, A.M. Kosmas, Inorg. Chem. 2005, 44, 8617-8627, (f) C.D. Antoniadis, S.K. Hadjikakou, N. Hadjiliadis, A. Papakyriakou, M. Baril, I.S. Butler, Chem. Eur. J. 2006, 12, 6888 – 6897, (g) C.D. Antoniadis, G.J. Corban, S.K. Hadjikakou, N. Hadjiliadis, Jin-Fang Meng, I.S. Butler, Bioinorg. Chem. App., 2006, Article ID 68542, (h) S.K. Hadjikakou, N. Hadjiliadis, Bioinorg. Chem. App., 2006, Article ID 60291, (i) I.-E. Parigoridi, G.J. Corban, S.K. Hadjikakou, N. Hadjiliadis, N. Kourkoumelis, G. Kostakis, V. Psycharis, C.P. Raptopoulou, M. Kubicki, Dalton Trans., 2008, 5159–5165, (j) A.M. Owczarzak, M. Kubicki, N. Kourkoumelis, S.K. Hadjikakou, RSC Advances, 2012, 2, 2856–2867, (k) G.J. Corban, C.D. Antoniadis, S.K. Hadjikakou, N. Kourkoumelis, V.Yu. Tyurin, A. Dolgano, E.R. Milaeva, M. Kubicki, P.V. Bernhardt, E.R.T. Tiekink, S. Skoulika, N. Hadjiliadis, Heteroatom Chem, 23, 2012, 498-511, (l) M. Biesiada, N. Kourkoumelis, M. Kubicki, A.M. Owczarzak, V. Balas S.K. Hadjikakou, Dalton Trans., 2014, 43, 4790–4806
12 T.L. Allen, R.M. Keeper, J. Am. Chem. Soc., 1953, 77, 2957-2960
13 P.H. Svensson, L. Kloo, Chem. Rev, 2003, 103, 1649-1684
14 S.S. Batsanov, Inorganic Materials, 37, 2001, 871–885. Translated from Neorganicheskie Materialy, 37, 2001, 1031–1046
15 F. Freeman, J.W. Zi1ler, H.N. Po, M.C. Keindl, J. Am. Chem. Soc. 1988, *110*, 2586-2591
16 G.S. Nichol, W. Clegg, Polyhedron 2006, 25, 1043-1056
17 K.H. Stone, S. Lapidus, P.W. Stephens, J. Appl. Crystallogr., 2009, 42, 385-391
18 D. Deme, A. Virion, J.L. Michot, J. Pommier, Arch. Biochem. Biophys., 1985, 236, 559-566

View Article Online
DOI: 10.1039/C7NJ01117B

19 (a) D.K. Bhattacharyya, U. Bandyopadhyay, R. Chatterjee, R.K. Banerjee, Biochem. J., 1993, 289, 575-580 (b) R.A. Copeland, Evaluation of Enzyme Inhibitors in Drug Discovery: A Guide for Medicinal Chemists and Pharmacologists, John Wiley & Sons, Inc., 2013
20 M.S. Kang, A.D. Elbein, Plant Physiol., 1983, 71, 551-554
21 I.H. Segel, "Biochemical Calculations," J. Wiley & Sons Inc., NY, second edn, 1976
22 M. Huwiler, H. Kohler, Eur. J. Biochem., 1984, 141, 69–474
23 R.P. Magnusson, A. Taurog, M.L. Dorris, J. Biol. Chem.,1984, 259, 13783–13790
24 M. Huwiler, U. Burgi, H. Kohler, Eur. J. Biochem., 1985, 147, 469–476
25 G.I. Berglund, G.H. Carlsson, A.T. Smith, H. Szoke, A. Henriksen, J. Hajdu, Nature, 2012, 417, 463-468
26 A. Henriksen, D.J. Schuller, K. Meno, K.G. Welinder, A.T. Smith, M. Gajhede, Biochemistry, 1998, 37, 8054-8060
27 L. M. Kabeya, A.A. de Marchi, A. Kanashiro, N.P. Lopes, C.H.T.P. da Silva, M.T. Pupo, Y.M. Lucisano-Valim, Bioorg Med Chem, 2007, 15, 1516-1524
28 Y.C. Chen, Trends Pharmacol Sci, 2015, 36, 78-95
29 M.A. Lill, M. Dobler, A. Vedani, Chemmedchem, 2006, 1, 73-81
30 P. Seal, J. Sikdar, A. Roy, R. Haldar, J Biomol Struct Dyn, 2016, 1-15
31 P. Daneshgar, A.A. Moosavi-Movahedi, P. Norouzi, M.R. Ganjali, A. Madadkar-Sobhani. A. A. Saboury, Int J Biol Macromol, 2009, 45, 129-134
32 A.C. Wallace, R.A. Laskowski, J. M. Thornton, Protein Eng, 1995, 8, 127-134
33 *CrystalClear*, Rigaku/MSC Inc., The Woodlands, Texas, USA, 2005
34 G.M. Sheldrick, Acta Cryst. 2008, A64, 112-122.
35 G.M. Sheldrick, Acta Cryst. 2015, C71, 3-8.
36 E. Krieger, G. Vriend, J Comput Chem., 2015, 36, 996-1007
37 O. Trott, A.J. Olson, J Comput Chem., 2010, 31, 455-461
38 E. Krieger, G. Vriend, Bioinformatics, 2014, 30, 2981-2982
39 E. Krieger, J.E. Nielsen, C.A.E.M. Spronk, G. Vriend, J. Mol. Graph. *Model.*, 2006, 25, 481-486
40 V. Hornak, R. Abel, A. Okur, B. Strockbine, A. Roitberg, C. Simmerling, Proteins, 2006, 65, 712-725
41 U. Essmann, L. Perera, M.L. Berkowitz, T. Darden, H. Lee, L.G. Pedersen, J Chem Phys, 1995, 103, 8577-8593

View Article Online
DOI: 10.1039/C7NJ01117B

Table 1. Hydrogen-bond geometry (Å, º) for **1**.

D—H···*A*	*D*—H	H···*A*	*D*···*A*	*D*—H···*A*
O2—H2*O*···O4	0.80 (4)	2.02 (4)	2.822 (3)	175 (4)
O4—H4*O*···I1	0.75 (3)	2.88 (3)	3.631 (2)	175 (3)
N1—H1···I3**	0.88	3.07	3.885 (2)	155
N2—H2···I2$^{!}$	0.88	2.82	3.699 (2)	173

Symmetry codes: -*z*; (**) -*x*+1, -*y*, -*z*; (!)-*x*+1/2, *y*+1, -*z*+1/2.

View Article Online
DOI: 10.1039/C7NJ01117B

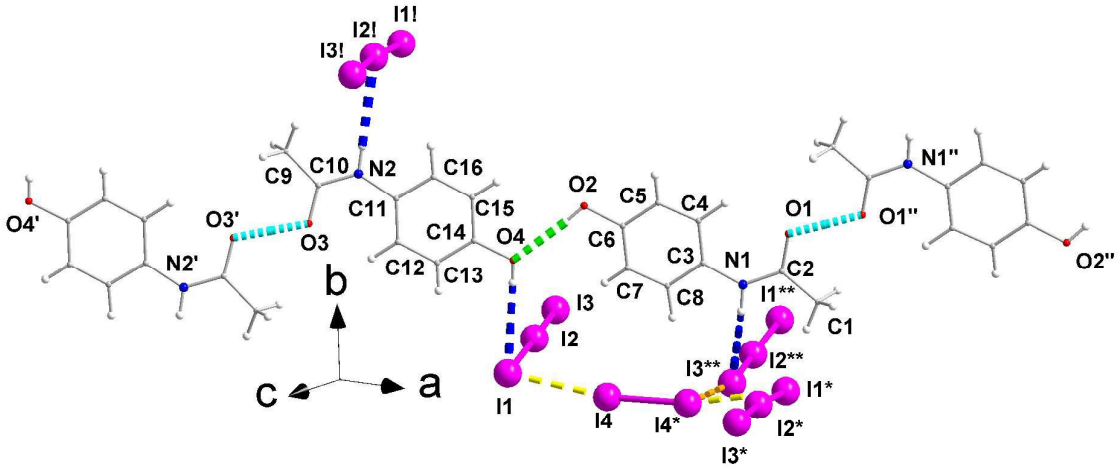

(A)

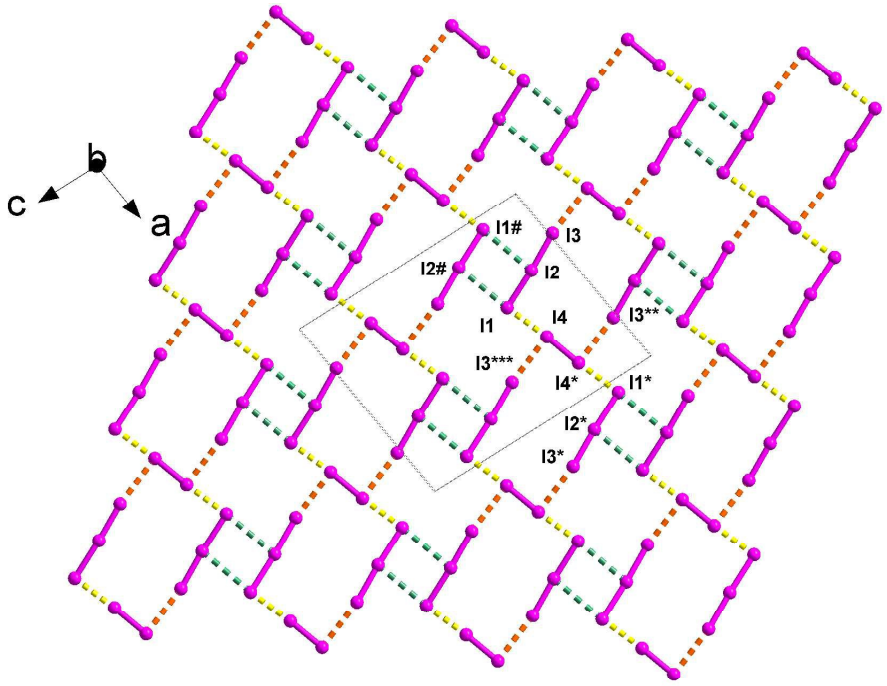

(B)

Figures 1. (A) Molecular diagram of compound **1** together with the atomic numbering scheme. Selected bond lengths (A) and angles [°]: I1-I2= 3.0076(5), I2-I3= 2.8494(5), I4-I4_a= 2.7509(4), O1-C2= 1.268(3), O2-C6= 1.365(4), O1-H1O= 1.2100, O2-H2O= 0.80(4), O3-C10= 1.257(3), O4-C14= 1.377(4), O3-H3O= 1.2100, O4-H4O= 0.76(4), N1-C2= 1.321(4), N1-C3= 1.434(4), C2-O1-H1O= 116.00, C6-O2-H2O= 112(3), C10-O3-H3O= 115.00, C14-O4-H4O= 114(3), I1-I2-I3= 175.84(1). Dashed cyan, green and blue lines indicate O3···H30···O3 (or O1···H1···O1), O2-H2O···O4 and O4-H4O···I1 and N1-H1N···I3 or N2-H2N···I2 hydrogen bonds. Dashed yellow, orange and green thick lines indicate I···I interaction of secondary bond, intermediate and weak van der Waals type interactions respectively in polyiodide unis. For the polyiodide interactions the colouring scheme given in (A) is followed in all figures.Symmetry code: (’): -x, 1-y, 1-z; (’’):2-x, 1-y,-z; (*): 1.5-x, y, 0.5-z; (**): 1-x, -y, -z; (***): 0.5+x, -y, 0.5+z; (!):0.5-x,1+y, 0.5-z, (#):0.5-x,y,0.5-z. (B) Polyiodide layers in the structure of **1** parallel to the (010) plane

View Article Online
DOI: 10.1039/C7NJ01117B

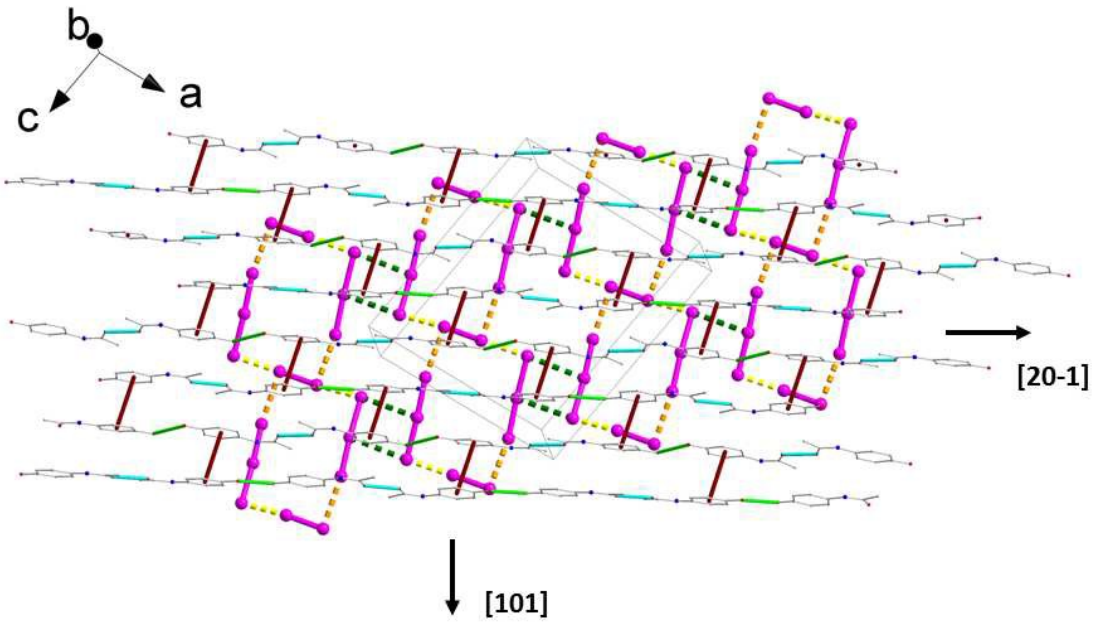

(A)

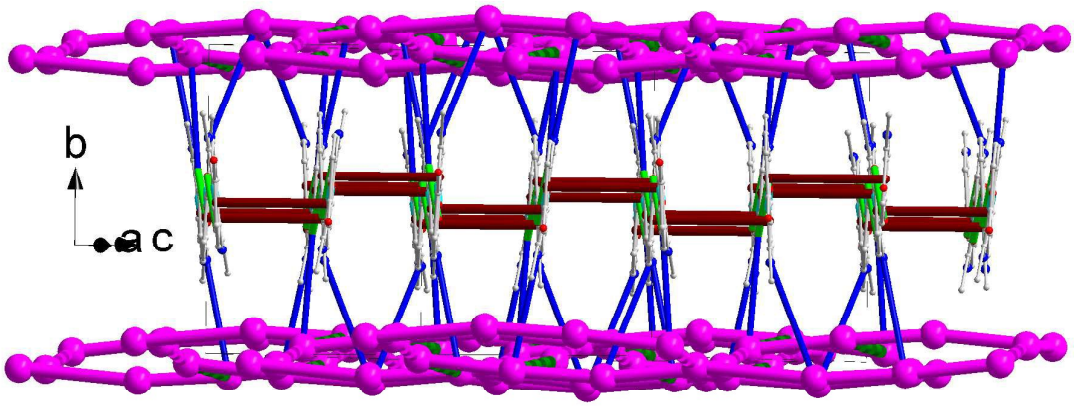

(B)

Figure 2.(A) Relative arrangements of PACET and polyiodide layers parallel to the (010) plane. The hydrogen bond inderaction of PACET molecules along the chains are indicated with green and light green thick lines for clarity reasons. The π-π interactions are also indicated with thick dark red lines. For the polyiodide interactions the colouring scheme given above is followed. (B) 3D architecture of **1** build through the stacking of polyodide and PACET layers along the b axis. The interlayer hydrogen bond interactions O4-H4O···I1, N1-H1N···I3 and N2-H2N···I2 are indicated with thick blue lines.

View Article Online
DOI: 10.1039/C7NJ01117B

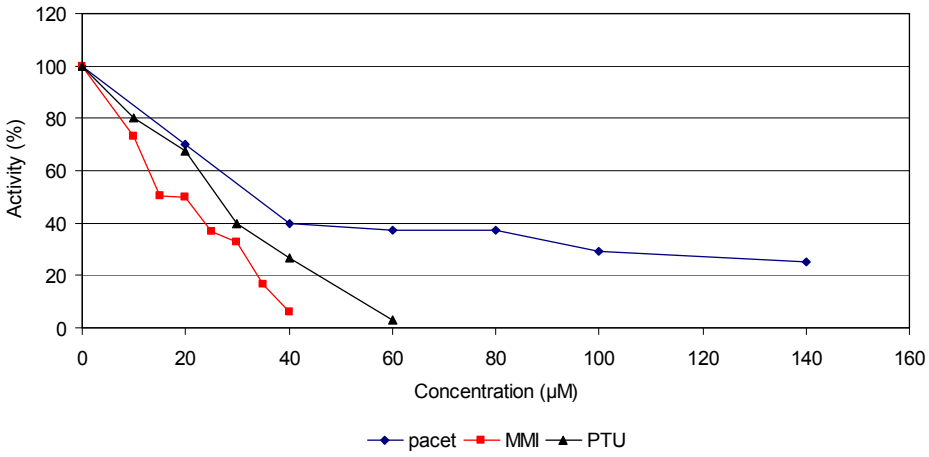

Figure 3. Peroxidase-catalysed iodide oxidation activity (A%) vs. various concentrations of paracetamol, MMI and PTU.

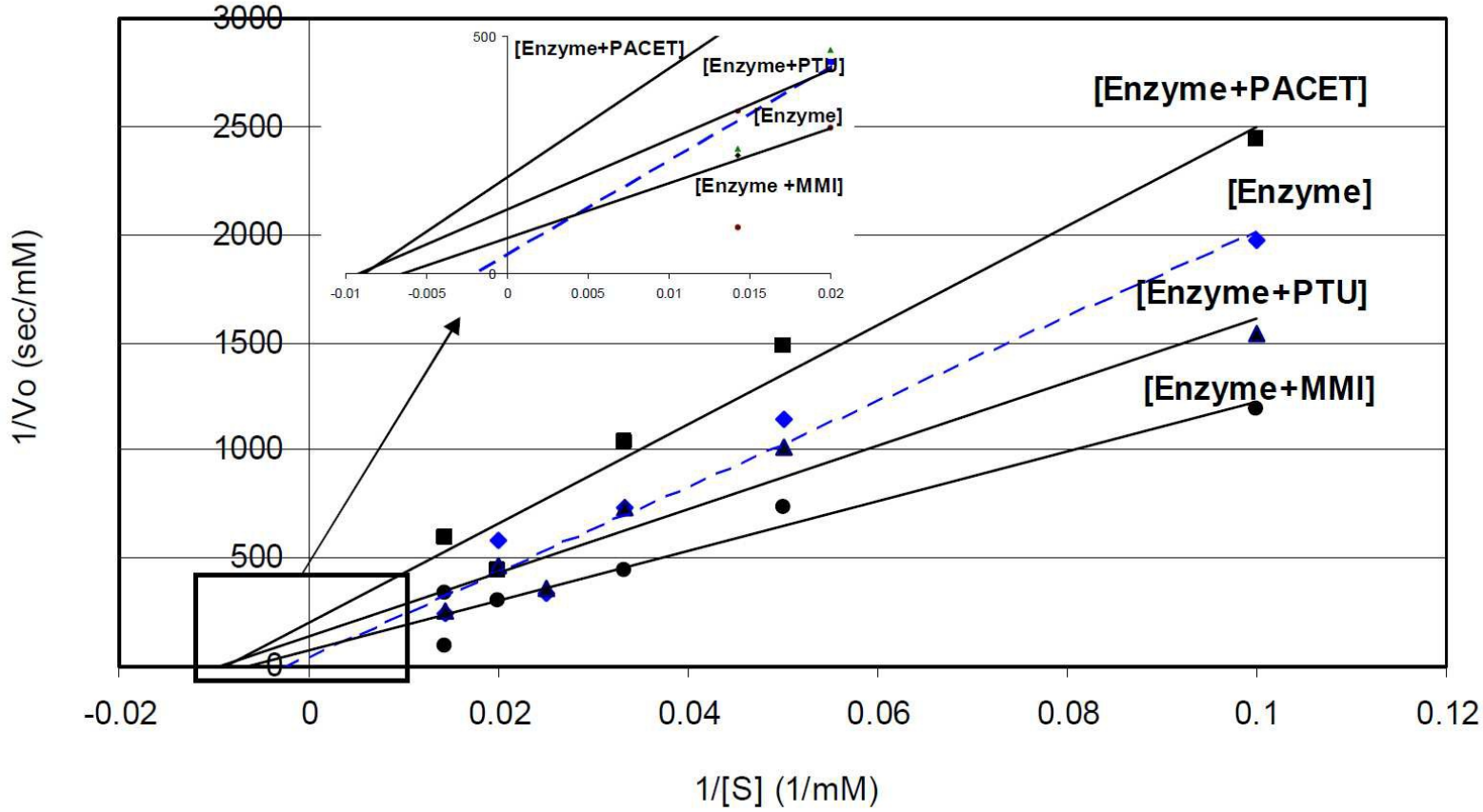

Figure 4. Graphical plotting for determination of K_m and V_{max} using Lineweaver–Burk coordinates for blank, PACET, MMI and PTU.

View Article Online
DOI: 10.1039/C7NJ01117B

Journal Name

ARTICLE

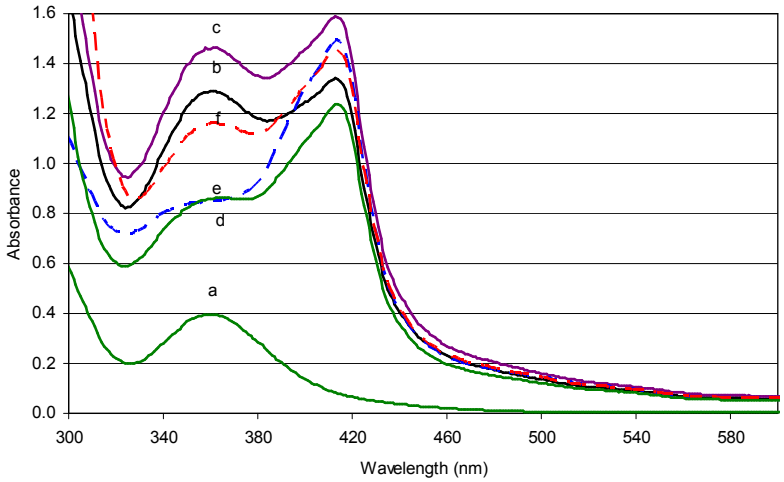

Figure 5. UV spectra of [a] KI + H_2O_2 [b] KI + H_2O_2 + FeTTPCl [c] KI + H_2O_2 + FeTTPCl + PACET [d] KI + H_2O_2 + FeTPPCl + Proline + PACET [e] KI + H_2O_2 + FeTTPCl + MMI [f] KI + H_2O_2 + FeTTPCl + PTU

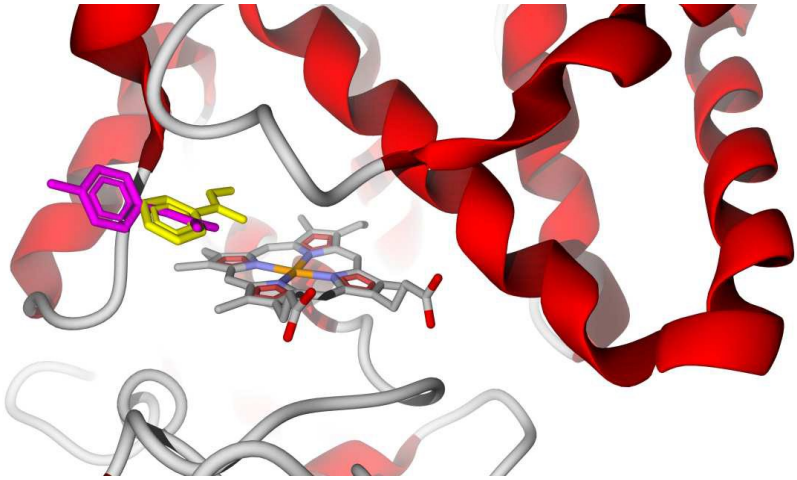

Figure 6. Top ranked docking pose of paracetamol (magenta) in unbound HRP structure superimposed to the HRP with benzhydroxamic acid as ligand (yellow)

View Article Online
DOI: 10.1039/C7NJ01117B

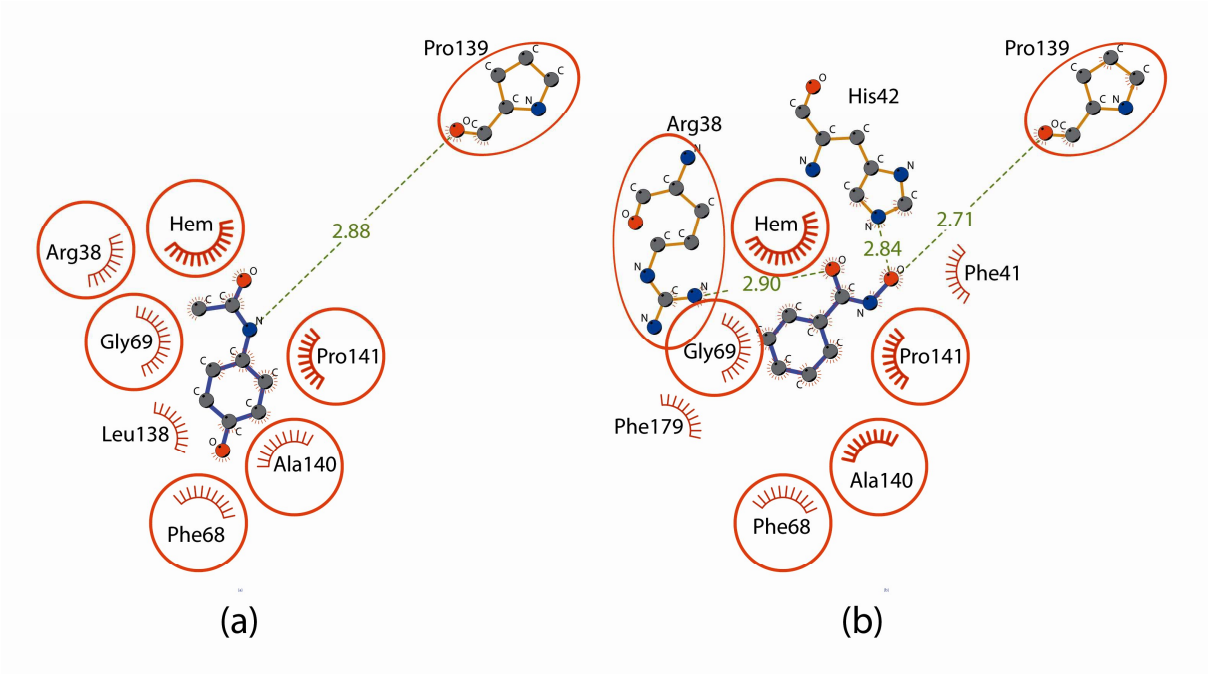

Figure 7. Schematic representation of the paracetamol (a) vs. BHA (b) binding in the active site of HRP generated by LigPlot+ [32]. Red circles and ellipses denote the similar residues environment.

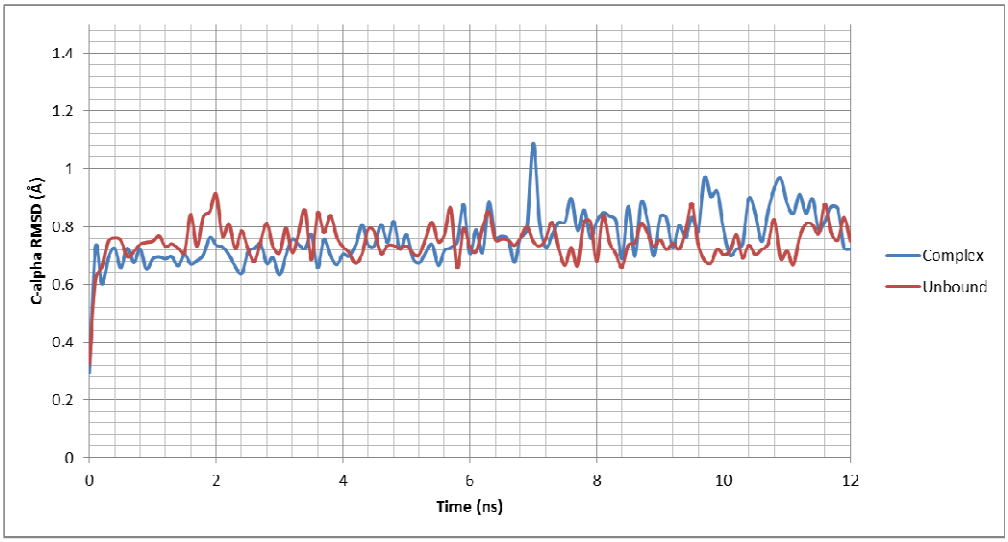

Figure 8. Root-mean-square deviation (RMSD) of Cα atoms relative to the energy minimized starting structure of HRP-paracetamol complex vs. Time